AAS 08-247

GEOMETRY OF OPTIMAL COVERAGE FOR TARGETS AGAINST A SPACE BACKGROUND SUBJECT TO VISIBILITY CONSTRAINTS

Belinda G. Marchand[1] and Christopher J. Kobel[2]

The optimal satellite coverage problem traditionally refers to maximizing the visibility of targets against an Earth background. In this study, the focus shifts to targets against a space background under certain constraints. Specifically, the goal of this study is to identify a systematic approach for determining the optimal altitude that maximizes sensor visibility of an area of space enclosed within an upper and lower target altitude range. It is further assumed that sensor visibility below the local horizon is diminished due to atmospheric or environmental factors. This environmental constraint is represented mathematically by optimizing the area covered above the local horizon but within the target altitude shells of interest for a fixed sensor range. In the course of this development, geometrical arguments are employed to identify an analytical expression for the coverage area. A graphical analysis tool, developed for this study, is employed in demonstrating the various geometrical arrangements and visualizing the optimal configurations.

INTRODUCTION

The goal of this study is the development of a systematic approach to identify the optimal satellite altitude needed to maximize the sensor visibility subject to a specific set of constraints. First, the targets of interest are assumed to exist above a lower and below an upper target altitude shell. Furthermore, it is assumed that the sensor capabilities are diminished by atmospheric and environmental factors. This is mathematically represented by constraining the area calculation to exclude the regions below the local horizon.

Traditionally, optimizing satellite coverage refers to maximizing the visibility of targets against an Earth background [1-2]. This is often referred to as the optimal "Below the Horizon" or "Below the Tangent Height" (BTH) coverage problem. Specifically, the optimal BTH coverage problem seeks to identify the minimum number of satellites required to achieve continuous coverage and maximize the visible area below the local horizon. The local horizon refers to an imaginary line that originates at the satellite and is tangent to the surface of the Earth, also referred to as the tangent line (TL). In the present investigation,

[1] Assistant Professor, The University of Texas at Austin, 210 E. 24th St., Austin, TX 78712; Member of the Technical Staff Senior, The Aerospace Corporation.
[2] Project Leader Senior, The Aerospace Corporation, 2350 E. El Segundo Blvd., M4-948, El Segundo, CA 90245.

however, the area of interest pertains to targets visible against a space background [3-4], termed "Above the Horizon" or "Above the Tangent Height" (ATH) coverage. Specifically, this investigation seeks to establish analytical means of maximizing the visible ATH coverage given sensor range constraints and a series of altitude bands. The approach presented is geometrical in nature. That is, geometrical arguments [5] are employed to establish an analytical expression for the coverage area and the optimal satellite altitude is identified numerically through a grid search of the solution space.

From this grid search, the optimal satellite height is easily identified for a given set of constraints. The results of the current investigation offer great insight into the evolution of the coverage area as a function of these parameters and constraints. The insight gained from these results serves as a stepping stone to more complex analyses involving additional constraints.

Traditional Methods for Optimal Coverage

As previously stated, the traditional problem of "optimal coverage" refers to maximizing the visibility of targets against an Earth background while minimizing the number of satellites in the constellation [2]. Identifying the satellite height that leads to maximum BTH coverage depends on the sensor capabilities. However, overall, the computation is straightforward. For instance, consider the illustration in Figure 1, where θ denotes the coverage angle, R represents the range shell (RS) radius, R_e is the Earth radius, and r_s denotes the radial distance from the center of the Earth to the satellite.

It is evident, from Figure 1, that the ground area covered by a single satellite is maximized when the coverage angle is maximized for a given sensor range. While the BTH problem focuses on targets against an Earth background, early studies into maximizing the visibility of targets against a space background led to investigations on how to maximize the ATH coverage are within a prescribed altitude shell [4]. To illustrate this, consider the image in Figure 2. In this case, r_{tar} represents the target altitude of interest, and r_t denotes the radius of the Tangent Height Shell (THS). The tangent height is an idealized version of the extent of the atmosphere, or any environmental elements that might diminish or interfere with the nominal visibility of the satellite target detection sensors. Thus, this concept is introduced as a means of incorporating these limitations in the present analysis.

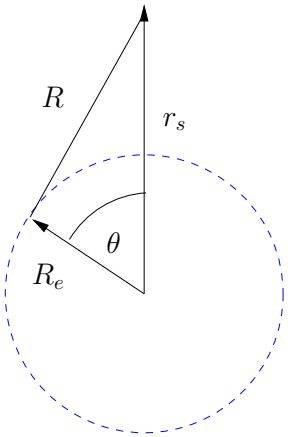

Figure 1 - BTH Coverage Geometry

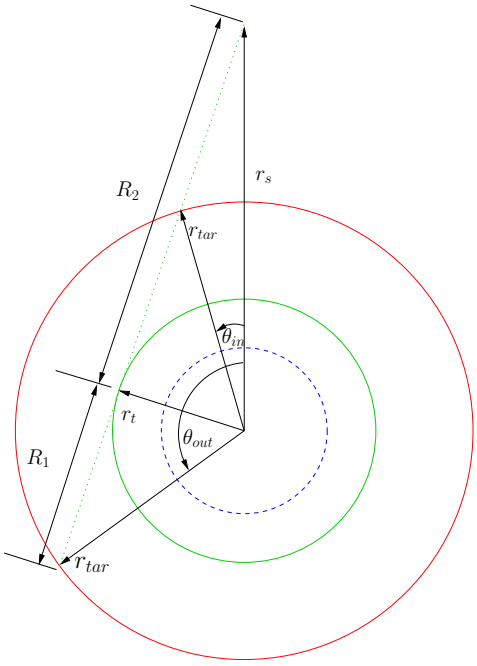

Figure 2 - ATH Coverage Geometry

For a fixed sensor range, idealized here as a spherical shell, optimizing the ATH coverage implies maximizing the volume that exists above the tangent height cone and below the target altitude shell. For simplicity, the present analysis is strictly two-dimensional and focuses on coverage area rather than coverage volume computations. However, it is understood that – due to the symmetry of the geometrical assumptions, the volume of coverage is simply the revolution of the coverage area by 360 degrees.

The orientation of the tangent line (TL) is determined by the satellite altitude. For a given target altitude and tangent height, it is possible to geometrically identify the minimum sensor range required for ATH coverage to exist, namely $R_2 - R_1$. Similarly, $R_1 + R_2$ represents the sensor range beyond which the coverage area reaches a plateau. This is evident from the variation in the shaded areas of Figure 3. Thus, in the traditional sense, maximum ATH coverage is achieved when the satellite altitude is selected such that $R = R_1 + R_2$. In the present study, the goal is to maximize ATH coverage within an altitude band defined by a lower altitude shell, r_l, and an upper altitude shell, r_u. Both of these shells exist above the tangent height shell. Thus, the problem is to maximize the area of intersection between the lower target altitude shell (LTAS), the upper target altitude shell (UTAS), the tangent line (TL), and the range shell (RS). In this case, the determination of the optimal satellite altitude is neither intuitive nor straightforward and requires additional consideration of the geometry of coverage.

SHELL INTERSECTIONS

The geometry of coverage depends on a number of key intersections defined by the problem parameters: satellite altitude, upper and lower target altitudes, tangent height, and sensor range. In the algorithm presented here, the calculation of the coverage area is a function of the location of these key intersections.

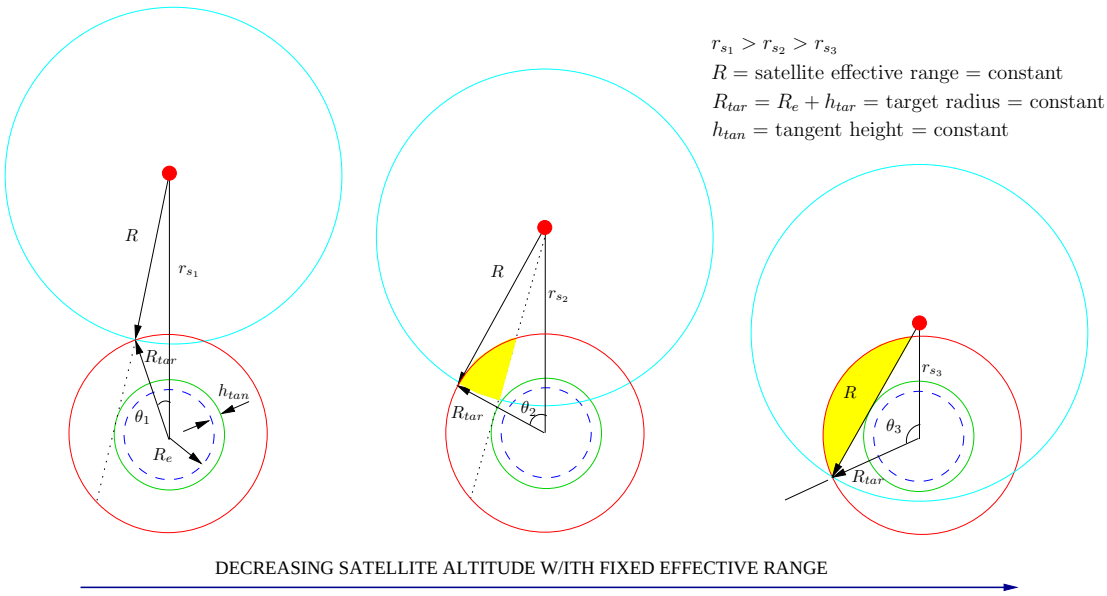

Figure 3 - Optimal ATH Coverage Geometry

The results of this study reveal that there is no single closed form equation that defines the coverage area. At best, a piecewise continuous function may be defined, but there are many special cases to consider that affect the calculations. Also, the representation of the coverage area is not unique, as there are multiple ways of decomposing the coverage geometry into fundamental components. Figure 4 illustrates a sample geometry that depicts one of the possible intersection scenarios. This illustration is useful in establishing the basic notation employed in this study.

The definitions for each of the key intersections possible are summarized in Table 1, and graphically illustrated in Figure 4. At most, 14 intersections are possible. The only intersections that are guaranteed to exist for all parameters are (T_1, T_2), (L_{1A}, L_{2A}), (U_{1A}, U_{2A}). The remaining intersections may or may not exist depending on the satellite altitude and the size of the RS. For example, (U_{1B}, U_{2B}) exist only if the satellite is above the UTAS. Similarly, (L_{1B}, L_{2B}) exist only if the satellite is above the LTAS. Also, (A_1, A_2) and (B_1, B_2) exist if the RS intersects the LTAS and UTAS, respectively. Naturally, it is possible to identify values of the satellite altitude and sensor range for which these intersections do not exist.

Table 1 – Description of Shell Intersections

Intersection	Description
U_{1A}, U_{2A}	The southern intersection of the TL with the UTAS
L_{1A}, L_{2A}	The southern intersection of the TL with the LTAS
L_{1B}, L_{2B}	The northern intersection of the TL with the LTAS
U_{1B}, U_{2B}	The northern intersection of the TL with the UTAS
T_1, T_2	The intersection of the TL with the RS
A_1, A_2	The intersection of the RS with the LTAS
B_1, B_2	The intersection of the RS with the UTAS

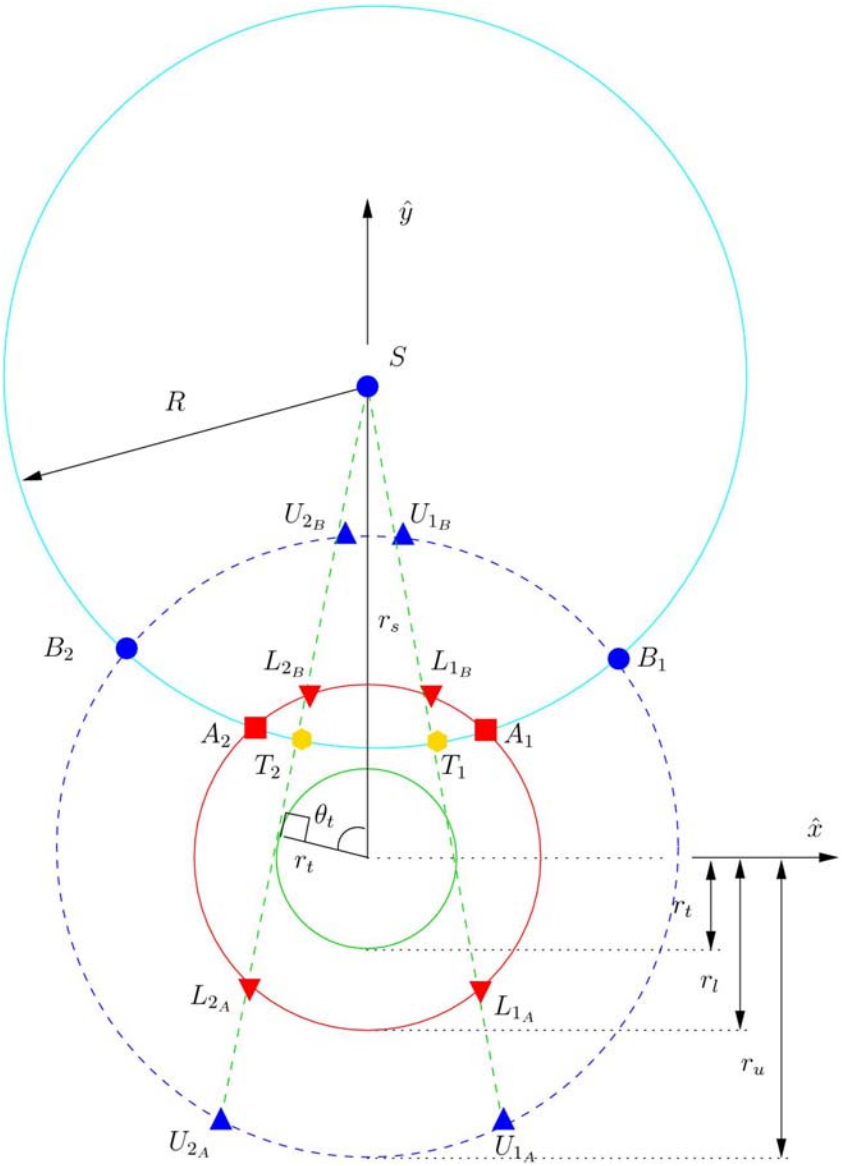

Figure 4 – Shell Intersections

As previously mentioned, the results of this study reveal that a piecewise continuous function may be identified to define the coverage area. The resulting composite function is continuous, though not necessarily smooth. As revealed by this investigation, the range of altitudes over which the function is smooth depends on where the RS intersects the TL and where that intersection (T_1, T_2) falls relative to the intersections of the LTAS and UTAS with the TL. This, in turn, depends on the satellite altitude and the size of the RS for a given UTAS, LTAS, and THS. The definitions of these intersections are employed in this study to define the coverage area associated with a given satellite altitude. A rotating coordinate system is selected for this determination such that the *y*-axis is the line from the center of the Earth to the satellite, and the *x*-axis is on the plane of the orbit of the satellite and perpendicular to the y-axis, as illustrated in Figure 4. As such, the location of the satellite in this rotating coordinate frame is given by $(x_s, y_s) = (0, r_s)$.

Intersections of RS with UTAS and LTAS

The intersection of the RS with the UTAS (B_1, B_2) is easily computed by simultaneously solving the mathematical relations that define the UTAS and the RS. At the point where the RS and UTAS intersect, the following equations must be satisfied,

$$x_{B_1}{}^2 + \left(y_{B_1} - r_s\right)^2 = R^2\,; \quad x_{B_1}{}^2 + y_{B_1}{}^2 = r_u{}^2 \tag{1}$$

The solution to this system of equations is given by

$$y_{B_1} = \frac{\left(r_u{}^2 + r_s{}^2 - R^2\right)}{2r_s}\,; \quad x_{B_1} = \sqrt{r_u{}^2 - y_{B_1}{}^2} \tag{2}$$

Of course, the symmetrical nature of the arrangement implies that

$$x_{B_2} = -x_{B_1}\,; \quad y_{B_2} = y_{B_1}\,. \tag{3}$$

A similar result applies for intersections at A_1 and A_2,

$$y_{A_1} = \frac{\left(r_l{}^2 + r_s{}^2 - R^2\right)}{2r_s}\,; \quad x_{A_1} = \sqrt{r_l{}^2 - y_{A_1}{}^2} \tag{4}$$

$$x_{A_2} = -x_{A_1}\,, y_{A_2} = y_{A_1}\,. \tag{5}$$

Intersections of the TL with the LTAS

The tangent line (TL) is defined by the position of the satellite $\left(x_s, y_s\right)$, and the point of intersection with the tangent height circle. The "coverage angle" associated with this point is defined, in Figure 4, as

$$\theta_t = \cos^{-1}\left(\frac{r_t}{r_s}\right). \tag{6}$$

Based on this definition, the slope of TL is given by,

$$m = \frac{y_t - y_s}{x_t - x_s}\,, \tag{7}$$

where,

$$x_t = r_t \sin\theta_t\,; \;\; y_t = r_t \cos\theta_t. \tag{8}$$

Let $\left(x_{L_{1A/B}}, y_{L_{1A/B}}\right)$ denote the cartesian coordinates of L_{1A} or L_{1B}. Then, the intersection of the LTAS with the TL is given by the solution to the following system of equations,

$$x_{L_{1A/B}}{}^2 + y_{L_{1A/B}}{}^2 = r_l^2\,; \quad y_{L_{1A/B}} = m\left(x_{L_{1A/B}} - x_s\right) + y_s \tag{9}$$

Since $x_s = 0$ and $y_s = r_s$, substitution of (7) into (9) leads to

$$\left(1 + m^2\right) x_{L_{1A/B}}{}^2 + 2mr_s x_{L_{1A/B}} + \left(r_s{}^2 - r_l{}^2\right) = 0\,. \tag{10}$$

The above quadratic is applicable to two different points, (A) and (B); thus, there are really a total of two quadratic equations. Only one of these equations is guaranteed to have a real set of solutions. The other may or may not have a solution, depending on whether or not the satellite is above the LTAS.

At a minimum, there are two solutions, $\left(x_{L_{1A}}, y_{L_{1A}}\right)$ and $\left(x_{L_{2A}}, y_{L_{2A}}\right)$, when the satellite is below the LTAS. However, there are four solutions $\left(x_{L_{1A}}, y_{L_{1A}}\right)$, $\left(x_{L_{2A}}, y_{L_{2A}}\right)$, $\left(x_{L_{1B}}, y_{L_{1B}}\right)$ and $\left(x_{L_{2B}}, y_{L_{2B}}\right)$, if the satellite is above the LTAS. For the right hand side intersections on Figure 4, it is clear that $m < 0$. Thus, if $r_s < r_l$ the southern intersection of the tangent line with the LTAS occurs when

$$x_{L_{1A}} = \frac{-2mr_s + \sqrt{4m^2 r_s^{\,2} - 4\left(1+m^2\right)\left(r_s^{\,2} - r_l^{\,2}\right)}}{2\left(1+m^2\right)}. \tag{11}$$

If $r_s > r_l$, a northern intersection exists and occurs at a smaller value of the $\underline{x}$-coordinate, namely

$$x_{L_{1B}} = \frac{-2mr_s - \sqrt{4m^2 r_s^{\,2} - 4\left(1+m^2\right)\left(r_s^{\,2} - r_l^{\,2}\right)}}{2\left(1+m^2\right)}. \tag{12}$$

In either case,

$$y_{L_{1A/B}} = m x_{L_{1A/B}} + r_s, \tag{13}$$

and

$$x_{L_{2A/B}} = -x_{L_{1A/B}}; \quad y_{L_{2A/B}} = y_{L_{1A/B}}. \tag{14}$$

Intersections of the TL with the UTAS

In the event the RS intersects the UTAS, the coordinates of intersection are easily identified by adapting equations (12) and (13) to the intersections with the UTAS,

$$x_{U_{1A}} = \frac{-2mr_s + \sqrt{4m^2 r_s^{\,2} - 4\left(1+m^2\right)\left(r_s^{\,2} - r_u^{\,2}\right)}}{2\left(1+m^2\right)}, \tag{15}$$

$$x_{U_{1B}} = \frac{-2mr_s - \sqrt{4m^2 r_s^{\,2} - 4\left(1+m^2\right)\left(r_s^{\,2} - r_u^{\,2}\right)}}{2\left(1+m^2\right)}, \tag{16}$$

$$y_{U_{1A/B}} = m x_{U_{1A/B}} + r_s. \tag{17}$$

Once again, symmetry implies that

$$x_{U_{2A/B}} = -x_{U_{1A/B}}; \quad y_{U_{2A/B}} = y_{U_{1A/B}}. \tag{18}$$

Intersections of the TL with the RS

The intersections of the TL with the RS are identified as T_1 and T_2. The cartesian coordinates of T_1 and T_2 are determined from the following system of equations,

$$x_{T_1}^{\,2} + \left(y_{T_1} - y_s\right)^2 = R^2; \quad y_{T_1} = m x_{T_1} + y_s. \tag{19}$$

The solution to this system of equations is determined as

$$x_{T_1} = \frac{R}{\sqrt{1+m^2}}; \quad y_{T_1} = m x_{T_1} + r_s \tag{20}$$

for

$$x_{T_2} = -x_{T_1}, \; y_{T_2} = y_{T_1}. \tag{21}$$

COMPOSITE COVERAGE AREA COMPONENTS

As previously mentioned, this study reveals that the coverage area cannot be reduced to a simple generalized equation. At best, a piecewise continuous function may be defined to assess the effective coverage area. The primary reason for this complication is that the definition of the coverage area equation changes with the location of the intersection points (T_1, T_2) relative to the intersection points $U_{1A/B}, U_{2A/B}, L_{1A/B}$, and $L_{2A/B}$. This, in turn, depends on a variety of factors including the satellite altitude, the sensor range, the LTAS, the UTAS, and the THS. To establish a systematic way of obtaining a piecewise continuous representation, the computation of the coverage area is divided into fundamental geometrical elements, mainly triangles, arc segments, and combinations thereof [5]. The effective coverage area is then constructed as a composite of these fundamental area elements. This section summarizes the coverage area of the fundamental shapes employed in constructing the piecewise continuous coverage area function.

Triangle

The coverage area function depends strongly on the Cartesian coordinates of each of the fundamental intersections previously defined. Thus, it is convenient to define the area of a triangle as a function of the semiperimeter because this quantity depends only on the lengths of each side of the triangle. The lengths of each side of a triangle are easily identified from Cartesian coordinates using the distance between vertices. The area of a triangle, $\mathbf{A}_{\triangle}$, in terms of the semiperimeter, is given by

$$\mathbf{A}_{\triangle}(a,b,c) = \sqrt{s(s-a)(s-b)(s-c)}, \tag{22}$$

where *a*, *b*, and *c* denote the lengths of each side and *s* is the semiperimeter,

$$s = \frac{(a+b+c)}{2}. \tag{23}$$

Arc Segment

The area of an arc segment, $\mathbf{A}_{\Sigma}$, is given by the difference between the area of a sector of a circle, and the area of a triangle as illustrated in Figure 5. The equation for the area of the arc segment illustrated in Figure 5 is given by

$$\mathbf{A}_{\Sigma}(r_u, c_{T_3}) = \underbrace{\frac{1}{2}\phi r_u^{\,2}}_{SECTOR} - \underbrace{\frac{c_{T_3} r_u}{2}\cos\frac{\phi}{2}}_{TRIANGLE}. \tag{24}$$

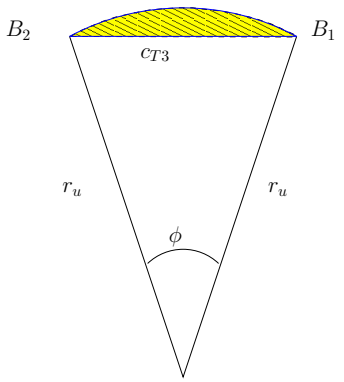

Figure 5 - Area of Arc Segment

In Figure 5, the angle ϕ is determined as

$$\phi = 2\sin^{-1}\left(\frac{c_{T_3}}{2r_u}\right), \tag{25}$$

Where c_{T_3} denotes the chord of the arc segment, and

$$\cos\frac{\phi}{2} = \frac{\sqrt{r_u^{\,2} - \left(\frac{c_{T_3}}{2}\right)^2}}{r_u} = \frac{\sqrt{4r_u^{\,2} - c_{T_3}^{\,2}}}{2r_u}. \tag{26}$$

Substitution of (25) and (26) into (24) leads to,

$$\mathbf{A}_{\Sigma}\left(r_u, c_{T_3}\right) = r_u^{\,2}\sin^{-1}\left(\frac{c_{T_3}}{2r_u}\right) - \frac{c_{T_3}}{4}\left(\sqrt{4r_u^{\,2} - c_{T_3}^{\,2}}\right). \tag{27}$$

Teardrop Sector

Traditionally, the area of a circular sector is defined as

$$\mathbf{A}_{\pi_1}\left(R, \overline{P_1P_2}\right) = \tfrac{1}{2}\lambda R^2, \tag{28}$$

where

$$\lambda = \cos^{-1}\left(\frac{\left|\overline{P_1P_2}\right|^2 - \left|\overline{P_1S}\right|^2 - \left|\overline{P_2S}\right|^2}{-2\left|\overline{P_1S}\right|\left|\overline{P_2S}\right|}\right) \tag{29}$$

denotes the angle interior to the sector, $\overline{P_1P_2}$ represents the chord, R is the radius of curvature, and S defines the origin. A geometrical object derived from the concept of a circular sector, is the teardrop pattern illustrated in Figure 6. In this case the shaded area is denoted $\mathbf{A}_{\pi_2}$. This type of pattern is useful over a certain range of parameters when computing the coverage area.

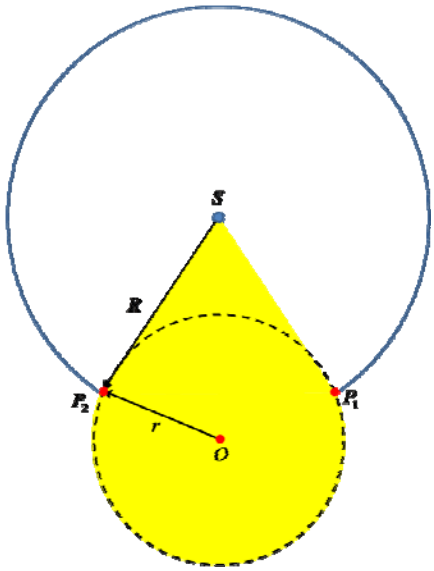

Figure 6 – Area of a Teardrop Pattern

The area of a teardrop pattern can be expressed as a sum of two fundamental components; a triangle and an arc segment, or its complement. In this case,

$$\mathbf{A}_{\pi_2}\left(r,R,\overline{P_1P_2}\right)=\begin{cases}\mathbf{A}_{\triangle}\left(R,\left|\overline{P_1P_2}\right|,R\right)+\mathbf{A}_{\Sigma}\left(r,\left|\overline{P_1P_2}\right|\right);\ \ R<\sqrt{r_s^{\,2}+r^2}\\ \mathbf{A}_{\triangle}\left(R,\left|\overline{P_1P_2}\right|,R\right)+\tilde{\mathbf{A}}_{\Sigma}\left(r,\left|\overline{P_1P_2}\right|\right);\ R\geq\sqrt{r_s^{\,2}+r^2}\end{cases}. \tag{30}$$

Composite Triangles

In the course of devising geometrical arguments to compute the area of coverage, two types of composite triangles are often encountered. In this case, a composite triangle refers to a three sided geometrical shape whose sides consist of any combination of line segments and spherical arcs.

Figure 7 illustrates one possible type of composite triangle that is sometimes encountered in the process of computing the effective coverage area. In this investigation, this type of composite triangle is denoted by Λ_1. These will be discussed in more detail in later sections.

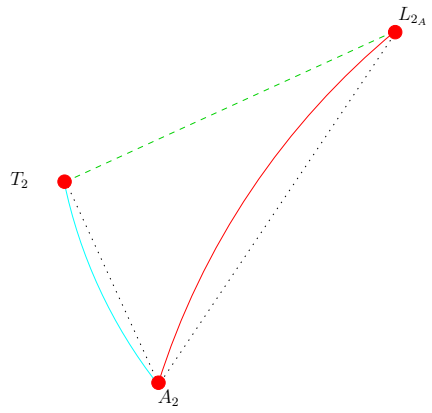

Figure 7 – Composite Triangle

In the example illustrated in

Figure 7, the radius of $\overset{\frown}{T_2L_2}$ is r_l, and the radius of $\overset{\frown}{B_2T_2}$ is R. The area, $\mathbf{A}_{\Lambda_1}$, of this composite triangle is a function of the areas of $\overset{\frown}{T_2L_2}$, $\overset{\frown}{B_2T_2}$, and the triangle defined by vertices B_2, T_2, and L_2. Since the Cartesian coordinates of these vertices are known, we find that,

$$\mathbf{A}_{\Sigma}\left(r_l,\overline{T_2L_2}\right)=r_l^{\,2}\sin^{-1}\left(\frac{\left|\overline{T_2L_2}\right|}{2r_l}\right)-\frac{\left|\overline{T_2L_2}\right|}{4}\left(\sqrt{4r_l^{\,2}-\left|\overline{T_2L_2}\right|^2}\right), \tag{31}$$

$$\mathbf{A}_{\Sigma}\left(R,\overline{B_2T_2}\right)=R^2\sin^{-1}\left(\frac{\left|\overline{B_2T_2}\right|}{2R}\right)-\frac{\left|\overline{B_2T_2}\right|}{4}\left(\sqrt{4R^2-\left|\overline{B_2T_2}\right|^2}\right), \tag{32}$$

$$\mathbf{A}_{\triangle}\left(\left|\overline{B_2T_2}\right|,\left|\overline{B_2L_2}\right|,\left|\overline{T_2L_2}\right|\right)=\sqrt{s\left(s-\left|\overline{B_2T_2}\right|\right)\left(s-\left|\overline{B_2L_2}\right|\right)\left(s-\left|\overline{T_2L_2}\right|\right)}, \tag{33}$$

Thus, the equation that describes the area of the composite triangle in

Figure 7 is given by

$$\begin{aligned}\mathbf{A}_{\Lambda_1}\left(r_l, R, \left|\overline{B_2T_2}\right|, \left|\overline{B_2L_2}\right|, \left|\overline{T_2L_2}\right|\right) = \mathbf{A}_{\triangle}\left(\left|\overline{B_2T_2}\right|, \left|\overline{B_2L_2}\right|, \left|\overline{T_2L_2}\right|\right) \\ - \mathbf{A}_{\Sigma}\left(r_l, \left|\overline{T_2L_2}\right|\right) + \mathbf{A}_{\Sigma}\left(R, \left|\overline{B_2T_2}\right|\right)\end{aligned}, \tag{34}$$

where,

$$s = \frac{1}{2}\left(\left|\overline{B_2T_2}\right| + \left|\overline{B_2L_2}\right| + \left|\overline{T_2L_2}\right|\right), \tag{35}$$

and

$$\left|\overline{B_2T_2}\right| = \sqrt{\left(x_{B_2} - x_{T_2}\right)^2 + \left(y_{B_2} - y_{T_2}\right)^2}, \tag{36}$$

$$\left|\overline{B_2L_2}\right| = \sqrt{\left(x_{B_2} - x_{L_2}\right)^2 + \left(y_{B_2} - y_{L_2}\right)^2}, \tag{37}$$

$$\left|\overline{T_2L_2}\right| = \sqrt{\left(x_{T_2} - x_{L_2}\right)^2 + \left(y_{T_2} - y_{L_2}\right)^2}. \tag{38}$$

Another type of composite triangle, Λ_2, is illustrated in Figure 8. This type of geometry is typically visible when the satellite crosses one of the target altitude shells, LTAS or UTAS. The area of the geometry illustrated below is determined as

$$\mathbf{A}_{\Lambda_2}\left(r_l, \left|\overline{L_2S}\right|, \left|\overline{L_1L_2}\right|, \left|\overline{L_1S}\right|\right) = \mathbf{A}_{\triangle}\left(\left|\overline{L_2S}\right|, \left|\overline{L_1L_2}\right|, \left|\overline{L_1S}\right|\right) - \mathbf{A}_{\Sigma}\left(r_l, \left|\overline{L_1L_2}\right|\right). \tag{39}$$

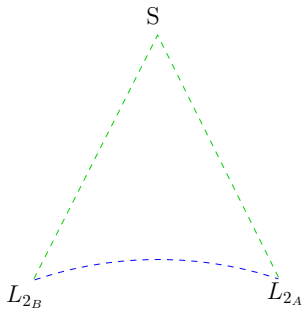

Figure 8 - Composite triangle

Intersection of Two Circles

Figure 9 illustrates one possible scenario for the area of intersection between the RS and the LTAS, $\mathbf{A}_{RS\cap LTAS}$. However, the formulation presented here is also applicable to the area of intersection between the RS and the UTAS, $\mathbf{A}_{RS\cap UTAS}$. For the intersection of the RS with the LTAS, $\left|\overline{OA_1}\right| = r_l$ and $\left|\overline{SA_1}\right| = R$. The shaded area Figure 9 is easily determined by computing the area of two arc segments, per the formula previously presented. Adapting equation(27) to this particular case yields,

$$\mathbf{A}_{RS\cap LTAS}\left(r_l, R, \left|\overline{A_1A_2}\right|\right) = \mathbf{A}_{\Sigma}\left(r_l, \left|\overline{A_1A_2}\right|\right) + \mathbf{A}_{\Sigma}\left(R, \left|\overline{A_1A_2}\right|\right). \tag{40}$$

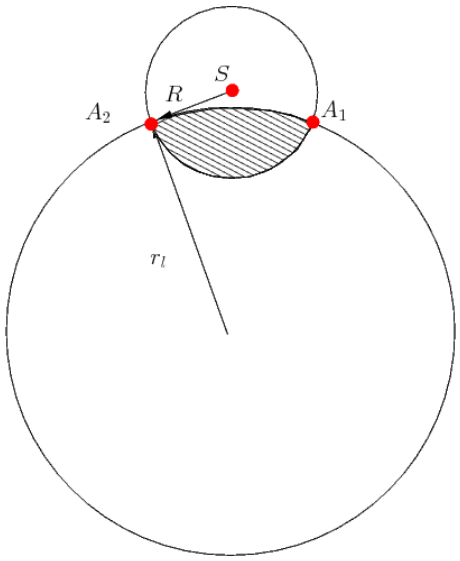

Figure 9 - Area of Intersection Between Two Circles

However, this equation is not applicable to all possible types of intersections between the two circular shells. The actual value of the coverage area depends on where the two circles intersect, and the location of these points relative to S and O. Figure 10 illustrates four possible cases relevant to this investigation that must be considered in computing the area of intersection between two circular shells. Figure 10(a) and Figure 10(b) illustrate the two possible scenarios for $R < r_l$, while Figure 10(c) and Figure 10(d) correspond to $R \geq r_l$. Figure 10(a) is further associated with $r_s > \sqrt{r_l^2 - R^2}$, while Figure 10(b) is associated with $r_s \leq \sqrt{r_l^2 - R^2}$. Similarly, Figure 10(c) corresponds to $r_s > \sqrt{R^2 - r_l^2}$, while Figure 10(d) implies $r_s \leq \sqrt{R^2 - r_l^2}$. Table 2 summarizes the general formula for the determination of the area of intersection between two circles, within the scope of the assumptions employed in this investigation.

CONDITION FOR NO COVERAGE

In defining the range of altitudes to consider, for a given set of parameters, it is only necessary to identify the minimum allowable satellite altitude and the altitude at which the satellite provides no ATH coverage. In this study, the minimum allowable altitude is defined as the tangent height. The maximum altitude of interest corresponds to the point at which $r_s > r_u$ while $T_1 = U_{1B}$ and $T_2 = U_{2B}$.

As observed from Figure 11, no part of the range circle exists within the UTAS and above the TL at or above this critical altitude, where the radial distance from the planet origin to the satellite is defined as r_{s_3}. Geometrically, this critical altitude is easily identified as,

$$r_{s_3} = \sqrt{\left(R + \sqrt{r_u^2 - r_t^2}\right)^2 + r_t^2} \ . \tag{41}$$

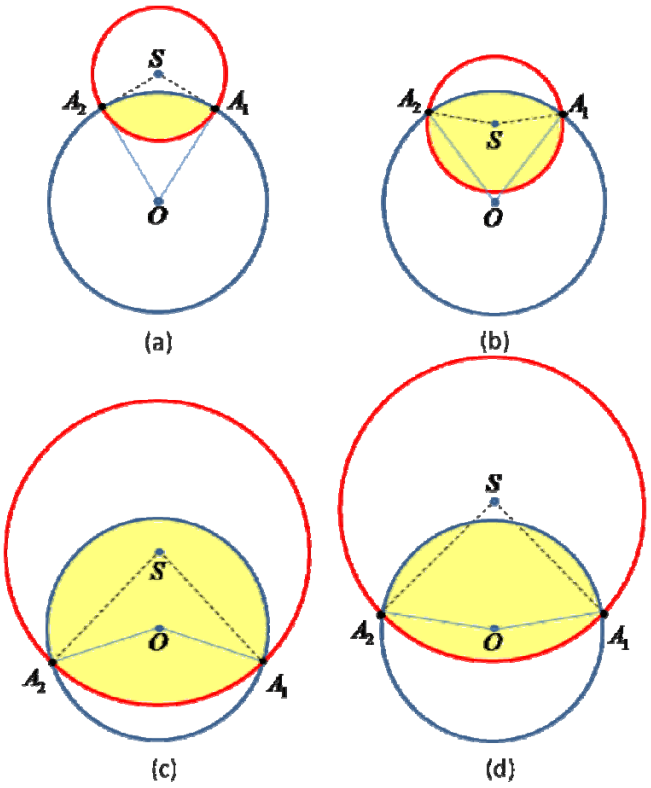

Figure 10 – Area of Intersection Between RS and LTAS

Table 2 – Area of Intersection of Two Circles

Condition	Area of Intersection
$\left(r_l > R \text{ and } r_s > \sqrt{r_l^2 - R^2}\right)$ or $\left(r_l \le R \text{ and } r_s > \sqrt{R^2 - r_l^2}\right)$	$\mathbf{A}_{RS\cap LTAS} = \mathbf{A}_{\Sigma}\left(R, \lvert\overline{A_1A_2}\rvert\right) + \mathbf{A}_{\Sigma}\left(r_l, \lvert\overline{A_1A_2}\rvert\right)$ (42)
$\left(r_l > R \text{ and } r_s \le \sqrt{r_l^2 - R^2}\right)$	$\mathbf{A}_{RS\cap LTAS} = \pi R^2 - \mathbf{A}_{\Sigma}\left(R, \lvert\overline{A_1A_2}\rvert\right) + \mathbf{A}_{\Sigma}\left(r_l, \lvert\overline{A_1A_2}\rvert\right)$ (43)
$\left(r_l \le R \text{ and } r_s \le \sqrt{R^2 - r_l^2}\right)$	$\mathbf{A}_{RS\cap LTAS} = \pi r_l^2 - \mathbf{A}_{\Sigma}\left(r_l, \lvert\overline{A_1A_2}\rvert\right) + \mathbf{A}_{\Sigma}\left(R, \lvert\overline{A_1A_2}\rvert\right)$ (44)

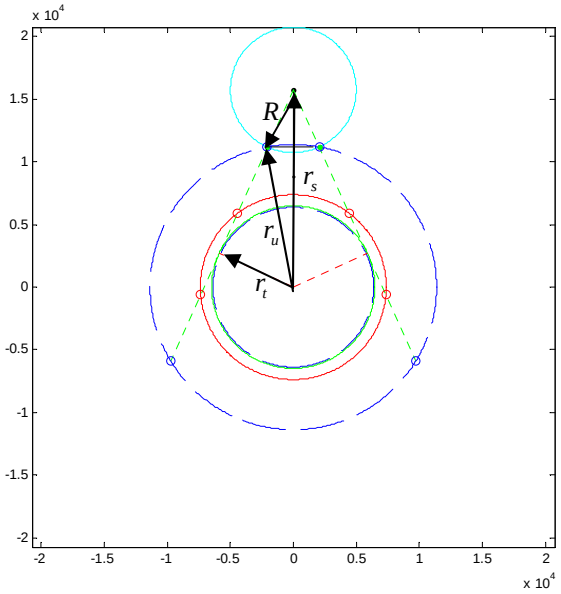

Figure 11 – Critical Altitude for no ATH coverage, for $r_s > r_u$

SINGLE SATELLITE ATH COVERAGE AREA

The table and images below summarize the calculation of the coverage area for all cases of interest. There are a total of 18 cases to consider in computing the coverage area, not including specific subcases introduced by equations (42)-(44). These are summarized in list form below. The symbol $\varnothing$ implies the quantity is empty, thus, $\left|\overline{A_1A_2}\right| = \varnothing$ implies that the RS does not intersect the LTAS and $\left|\overline{B_1B_2}\right| = \varnothing$ implies the RS does not intersect the UTAS. Note that there is no unique way of representing the coverage area for a specific case. Thus, the results presented here represent one possible representation, though care was taken in selecting a formulation that would simplify the calculations while allowing for a systematic approach to constructing the piecewise continuous coverage area function.

When the satellite is below the LTAS and above the THS, the function that describes the coverage area can be divided into three segments: $\left|\overline{T_2S}\right| < \left|\overline{L_{2A}S}\right|$, $\left|\overline{L_{2A}S}\right| \le \left|\overline{T_2S}\right| < \left|\overline{U_{2A}S}\right|$, and $\left|\overline{U_{2A}S}\right| \le \left|\overline{T_2S}\right|$. Even within each of these three cases, the calculation of the coverage area needs to be adjusted according to the conditions defined in Table 3. Thus, the coverage area function, for $r_t \le r_s < r_l$, can take on up to five different forms; 1(a), 1(b.i), 1(b.ii), 1(c.i), and 1(c.ii). Table 4 and Table 5 illustrate a similar relation for $r_l \le r_s < r_u$ and $r_u \le r_s < r_{s_3}$. Based on the conditions in Table 3 through Table 5 the composite piecewise continuous coverage area functions, for each of the three possible altitude ranges, are summarized in Table 6 through Table 8.

Table 3 – Coverage Area Subcases for $r_t \le r_s < r_l$

$\left\|\overline{T_2S}\right\| < \left\\|\overline{L_{2A}S}\right\|$	$\left\|\overline{L_{2A}S}\right\| \le \left\|\overline{T_2S}\right\| < \left\|\overline{U_{2A}S}\right\|$	$\left\|\overline{U_{2A}S}\right\| \le \left\|\overline{T_2S}\right\|$
1(a)	1 (b.i): $\left\|\overline{A_1A_2}\right\| \ne \varnothing$ 1 (b.ii): $\left\|\overline{A_1A_2}\right\| = \varnothing$	1 (c.i): $\left\|\overline{A_1A_2}\right\| \ne \varnothing$ 1 (c.ii): $\left\|\overline{A_1A_2}\right\| = \varnothing$

Table 4 - Coverage Area Subcases for $r_l \le r_s < r_u$

$\lvert\overline{T_2S}\rvert < \lvert\overline{L_{2B}S}\rvert$	$\lvert\overline{L_{2B}S}\rvert \le \lvert\overline{T_2S}\rvert < \lvert\overline{L_{2A}S}\rvert$	$\lvert\overline{L_{2A}S}\rvert \le \lvert\overline{T_2S}\rvert < \lvert\overline{U_{2A}S}\rvert$	$\lvert\overline{U_{2A}S}\rvert \le \lvert\overline{T_2S}\rvert$
2(a)	2(b)	2(c.i): $\lvert\overline{A_1A_2}\rvert \neq \varnothing$	2(d.i): $\lvert\overline{A_1A_2}\rvert \neq \varnothing$
		2(c.ii) $\lvert\overline{A_1A_2}\rvert = \varnothing$	2(d.ii): $\lvert\overline{A_1A_2}\rvert = \varnothing$

Table 5 - Coverage Area Subcases for $r_u \le r_s < r_{s_3}$

$\lvert\overline{T_2S}\rvert < \lvert\overline{U_{2B}S}\rvert$	$\lvert\overline{U_{2B}S}\rvert \le \lvert\overline{T_2S}\rvert < \lvert\overline{L_{2B}S}\rvert$	$\lvert\overline{L_{2B}S}\rvert \le \lvert\overline{T_2S}\rvert < \lvert\overline{L_{2A}S}\rvert$	$\lvert\overline{L_{2A}S}\rvert \le \lvert\overline{T_2S}\rvert < \lvert\overline{U_{2A}S}\rvert$	$\lvert\overline{U_{2A}S}\rvert \le \lvert\overline{T_2S}\rvert$
3(a)	3(b)	3(c)	3(d.i): $\lvert\overline{A_1A_2}\rvert \neq \varnothing$	3(e.i): $\lvert\overline{A_1A_2}\rvert \neq \varnothing$
			3(d.ii): $\lvert\overline{A_1A_2}\rvert = \varnothing$	3(e.ii): $\lvert\overline{A_1A_2}\rvert = \varnothing$

Table 6 – Coverage Area for $r_t \le r_s < r_l$

Case	Area
1(a)	$\mathbf{A} = \mathbf{A}_{UTAS \cap RS} - \mathbf{A}_{LTAS \cap RS}$
1(b.i)	$\mathbf{A} = \mathbf{A}_{UTAS \cap RS} - \mathbf{A}_{LTAS \cap RS} - 2\mathbf{A}_{\Lambda_1}\left(R, r_l, \lvert\overline{T_2L_{2A}}\rvert, \lvert\overline{T_2A_2}\rvert, \lvert\overline{A_2L_{2A}}\rvert\right)$
1(b.ii)	$\mathbf{A} = \mathbf{A}_{UTAS \cap RS} - \pi r_l^2 - \mathbf{A}_{\pi_1}\left(R, \lvert\overline{T_1T_2}\rvert\right) + \mathbf{A}_{\pi_2}\left(r_l, R, \lvert\overline{L_{1A}L_{2A}}\rvert\right)$
1 (c.i)	$\mathbf{A} = \mathbf{A}_{UTAS \cap RS} - \mathbf{A}_{LTAS \cap RS} - 2\mathbf{A}_{\Lambda_1}\left(r_l, R, \lvert\overline{T_2L_{2A}}\rvert, \lvert\overline{T_2A_2}\rvert, \lvert\overline{A_2L_{2A}}\rvert\right) + 2\mathbf{A}_{\Lambda_1}\left(r_u, R, \lvert\overline{T_2U_{2A}}\rvert, \lvert\overline{T_2B_2}\rvert, \lvert\overline{B_2U_{2A}}\rvert\right)$
1 (c.ii)	$\mathbf{A} = \pi r_u^{\,2} - \pi r_l^2 - \mathbf{A}_{\pi_2}\left(r_u, R, \lvert\overline{U_{1A}U_{2A}}\rvert\right) + \mathbf{A}_{\pi_2}\left(r_l, R, \lvert\overline{L_{1A}L_{2A}}\rvert\right)$

Table 7 – Coverage Area for $r_l \le r_s < r_u$

Case	Area
2(a)	$\mathbf{A} = \mathbf{A}_{UTAS \cap RS} - \mathbf{A}_{\pi_1}\left(R, \left\|\overline{T_1T_2}\right\|\right)$
2(b)	$\mathbf{A} = \mathbf{A}_{UTAS \cap RS} - \mathbf{A}_{LTAS \cap RS} - \mathbf{A}_{\Lambda_2}\left(r_l, \left\|\overline{L_{1B}S}\right\|, \left\|\overline{L_{1B}L_{2B}}\right\|, \left\|\overline{L_{2B}S}\right\|\right)$
2(c.i)	$\mathbf{A} = \mathbf{A}_{UTAS \cap RS} - \mathbf{A}_{LTAS \cap RS} - \mathbf{A}_{\Lambda_2}\left(r_l, \left\|\overline{L_{1B}S}\right\|, \left\|\overline{L_{1B}L_{2B}}\right\|, \left\|\overline{L_{2B}S}\right\|\right) - 2\mathbf{A}_{\Lambda_1}\left(r_l, R, \left\|\overline{T_2L_{2A}}\right\|, \left\|\overline{T_2A_2}\right\|, \left\|\overline{A_2L_{2A}}\right\|\right)$
2(c.ii)	$\mathbf{A} = \mathbf{A}_{UTAS \cap RS} - \mathbf{A}_{LTAS \cap RS} - \mathbf{A}_{\Lambda_2}\left(r_l, \left\|\overline{L_{1B}S}\right\|, \left\|\overline{L_{1B}L_{2B}}\right\|, \left\|\overline{L_{2B}S}\right\|\right) - \mathbf{A}_{\pi_1}\left(R, \left\|\overline{T_1T_2}\right\|\right) + \mathbf{A}_{\pi_2}\left(r_l, R, \left\|\overline{L_{1A}L_{2A}}\right\|\right)$
2(d.i)	$\mathbf{A} = \mathbf{A}_{UTAS \cap RS} - \mathbf{A}_{LTAS \cap RS} - \mathbf{A}_{\Lambda_2}\left(r_l, \left\|\overline{L_{1B}S}\right\|, \left\|\overline{L_{1B}L_{2B}}\right\|, \left\|\overline{L_{2B}S}\right\|\right) - 2\mathbf{A}_{\Lambda_1}\left(r_l, R, \overline{T_2L_{2A}}, \overline{T_2A_2}, \overline{A_2L_{2A}}\right)$ $\mathbf{A} = \mathbf{A} + 2\mathbf{A}_{\Lambda_1}\left(r_u, R, \overline{T_2U_{2A}}, \overline{T_2B_2}, \overline{B_2U_{2A}}\right)$
2(d.ii)	$\mathbf{A} = \pi r_u^{\,2} - \pi r_l^{\,2} - \mathbf{A}_{\pi_2}\left(r_u, R, \left\|\overline{U_{1A}U_{2A}}\right\|\right) + \mathbf{A}_{\pi_2}\left(r_l, R, \left\|\overline{L_{1A}L_{2A}}\right\|\right) - \mathbf{A}_{\Lambda_2}\left(r_l, \left\|\overline{L_{1B}S}\right\|, \left\|\overline{L_{1B}L_{2B}}\right\| \left\|\overline{L_{2B}S}\right\|\right)$

Table 8 - Coverage Area for $r_l \le r_s < r_u$

Case	Area
3(a)	$\mathbf{A} = \mathbf{0}$
3(b)	$\mathbf{A} = \mathbf{A}_{UTAS \cap RS} - \mathbf{A}_{\pi_1}\left(R, \left\|\overline{T_1T_2}\right\|\right) + \mathbf{A}_{\Lambda_2}\left(r_u, \overline{U_{2B}S}, \overline{U_{1B}U_{2B}}, \overline{U_{1B}S}\right)$
3(c)	$\mathbf{A} = \mathbf{A}_{UTAS \cap RS} - \mathbf{A}_{\Lambda_2}\left(r_l, \left\|\overline{L_{1B}S}\right\|, \left\|\overline{L_{1B}L_{2B}}\right\|, \left\|\overline{L_{2B}S}\right\|\right) + \mathbf{A}_{\Lambda_2}\left(r_u, \left\|\overline{U_{1B}S}\right\|, \left\|\overline{U_{1B}U_{2B}}\right\|, \left\|\overline{U_{2B}S}\right\|\right)$
3(d.i)	$\mathbf{A} = \mathbf{A}_{UTAS \cap RS} - \mathbf{A}_{\Lambda_2}\left(r_l, \left\|\overline{L_{1B}S}\right\|, \left\|\overline{L_{1B}L_{2B}}\right\|, \left\|\overline{L_{2B}S}\right\|\right) + \mathbf{A}_{\Lambda_2}\left(r_u, \left\|\overline{U_{1B}S}\right\|, \left\|\overline{U_{1B}U_{2B}}\right\|, \left\|\overline{U_{2B}S}\right\|\right)$ $\mathbf{A} = \mathbf{A} - 2\mathbf{A}_{\Lambda_1}\left(r_l, R, \left\|\overline{T_2L_{2A}}\right\|, \left\|\overline{T_2A_2}\right\|, \left\|\overline{A_2L_{2A}}\right\|\right)$
3(d.ii)	$\mathbf{A} = \mathbf{A}_{UTAS \cap RS} - \pi r_l^{\,2} - \mathbf{A}_{\Lambda_2}\left(r_l, \left\|\overline{L_{1B}S}\right\|, \left\|\overline{L_{1B}L_{2B}}\right\|, \left\|\overline{L_{2B}S}\right\|\right) + \mathbf{A}_{\Lambda_2}\left(r_u, \left\|\overline{U_{1B}S}\right\|, \left\|\overline{U_{1B}U_{2B}}\right\|, \left\|\overline{U_{2B}S}\right\|\right) - \mathbf{A}_{\pi_1}\left(R, \left\|\overline{T_1T_2}\right\|\right)$ $\mathbf{A} = \mathbf{A} + \mathbf{A}_{\pi_2}\left(r_l, R, \overline{L_{1A}L_{2A}}\right)$
3(e.i)	$\mathbf{A} = \mathbf{A}_{UTAS \cap RS} - \mathbf{A}_{LTAS \cap RS} - \mathbf{A}_{\Lambda_2}\left(r_l, \left\|\overline{L_{1B}S}\right\|, \left\|\overline{L_{1B}L_{2B}}\right\|, \left\|\overline{L_{2B}S}\right\|\right) + \mathbf{A}_{\Lambda_2}\left(r_u, \left\|\overline{U_{1B}S}\right\|, \left\|\overline{U_{1B}U_{2B}}\right\|, \left\|\overline{U_{2B}S}\right\|\right)$ $\mathbf{A} = \mathbf{A} - 2\mathbf{A}_{\Lambda_1}\left(r_l, R, \left\|\overline{T_2L_{2A}}\right\|, \left\|\overline{T_2A_2}\right\|, \left\|\overline{A_2L_{2A}}\right\|\right) + 2\mathbf{A}_{\Lambda_1}\left(r_u, R, \left\|\overline{T_2U_{2A}}\right\|, \left\|\overline{T_2B_2}\right\|, \left\|\overline{B_2U_{2A}}\right\|\right)$
3(e.ii)	$\mathbf{A} = \pi r_u^{\,2} - \pi r_l^{\,2} - \mathbf{A}_{\pi_2}\left(r_u, R, \overline{U_{1A}U_{2A}}\right) + \mathbf{A}_{\pi_2}\left(r_l, R, \overline{L_{1A}L_{2A}}\right) - \mathbf{A}_{\Lambda_2}\left(r_l, \left\|\overline{L_{1B}S}\right\|, \left\|\overline{L_{1B}L_{2B}}\right\|, \left\|\overline{L_{2B}S}\right\|\right)$ $\mathbf{A} = \mathbf{A} + \mathbf{A}_{\Lambda_2}\left(r_u, \left\|\overline{U_{1B}S}\right\|, \left\|\overline{U_{1B}U_{2B}}\right\|, \left\|\overline{U_{2B}S}\right\|\right)$

The coverage area associated with each of these cases is illustrated in Figure 14. To demonstrate how one arrives at each of the equations in Table 6 through Table 8, consider case 2(d.i). The coverage area equation for case 2(d.i) can be decomposed into several area elements, including $\mathbf{A}_{UTAS \cap RS}$, $\mathbf{A}_{LTAS \cap RS}$, $\mathbf{A}_{\Lambda_2}$, and $\mathbf{A}_{\Lambda_1}$. Figure 15 illustrates how the composite total coverage area is constructed from these elements. The contents of Table 6 through Table 8 define an objective function to an optimization process that seeks to identify the optimal altitude that maximizes the constrained ATH coverage area. An example of this process is presented in the next set of examples.

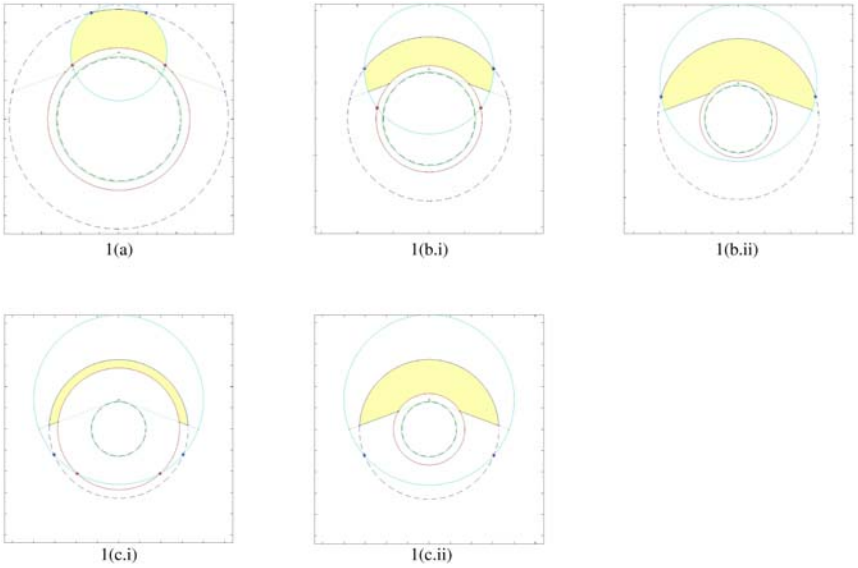

Figure 12 - Case 1 Scenarios

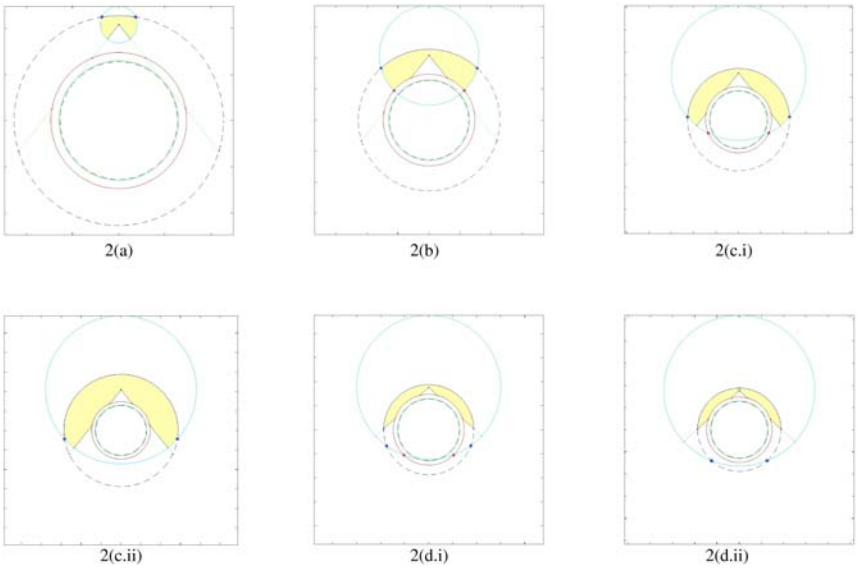

Figure 13 - Case 2 Scenarios

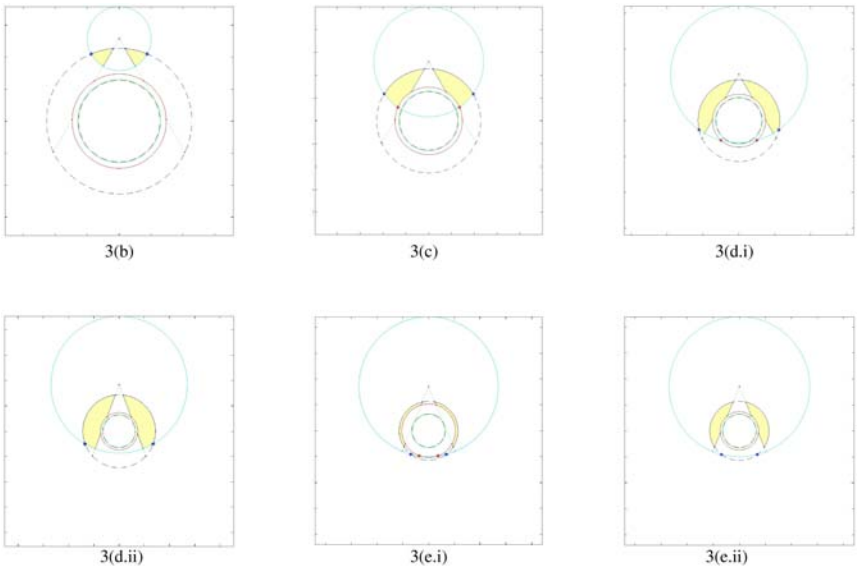

Figure 14 - Case 3 Scenarios

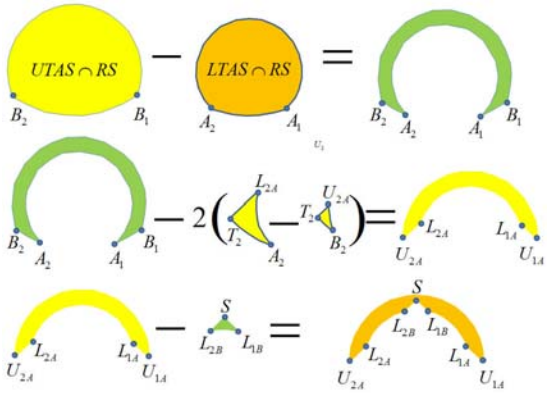

Figure 15 - Coverage Area Calculation for Case 2(d.i)

EXAMPLE 1

Figure 16(a) depicts the coverage area as a function of satellite altitude for a fixed sensor range. As expected, the coverage area is nullified as $r \to r_{s_3}$. In this particular example, the maximum coverage area is achieved when the satellite altitude is 1353 km, for R = 5000 km, h_l = 1000 km, h_u = 5000 km, and h_t = 100 km. The corresponding geometrical configuration is illustrated in Figure 16(b). It is interesting to note that, unlike the BTH case, maximizing θ does not lead to maximum coverage area. Also, unlike the traditional ATH case, $R_1 + R_2$ does not offer the maximum coverage area for a fixed altitude band. In fact, the results of this study indicate that there is no obvious relation between the coverage angle and the maximum coverage area. Thus, the methodology presented here is an important step towards identifying optimal constellations for maximum ATH altitude band limited coverage, and also for the future inclusion of additional constraints.

EXAMPLE 2

A more complete analysis of the optimal solutions pace is presented in Figure 17 (a-b). These figures depict contours of optimal satellite altitude as a function of sensor range and upper target altitude. In this particular example, the lower target altitude is held fixed at 600 km to simplify the visualization of the optimal altitude trends. Figure 17(b) is of particular interest as it reveals two ridge lines that separate the central region of the contours from the exterior regions. Numerical examination of these ridge lines reveals that the lower ridge line corresponds to the set of optimal solutions associated with a critical intersection between L2a, T2, and A2. By symmetry, at that same altitude, there is also an intersection between L1a, T1, and A1. Similarly, the upper ridge line is representative of optimal solutions associated with the critical intersection of U2a, T2, and B2.

It is interesting to note that, in the exterior regions outlined by these ridge lines, the relation between the maximum coverage area and the sensor and upper target altitudes, seems relatively linear, unlike that observed in the interior region. While the significance of these trends is of interest for future investigations, it is not the focus of the present study. Every design problem is linked to a different set of constraints and parameters, all of which affect the trends outlined in these Figures. Thus, it would be premature to draw any globally definitive conclusions from these results. However, the results presented here do offer a proof of concept for the proposed methodology. The algorithm and graphical tools presented are an important first step towards the future goals of this study. Specifically, the development of algorithms that can assist the designer in identifying the minimum number of satellites and the optimal arrangement required to maximize the coverage of targets against a space background over a prespecified altitude and latitude band.

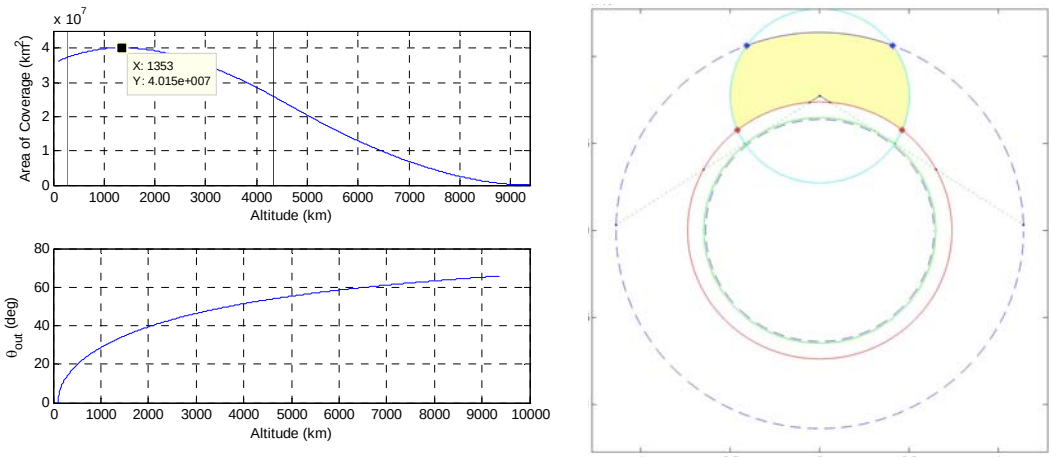

(a) (b)

Figure 16 – ATH Coverage Area vs. Altitude

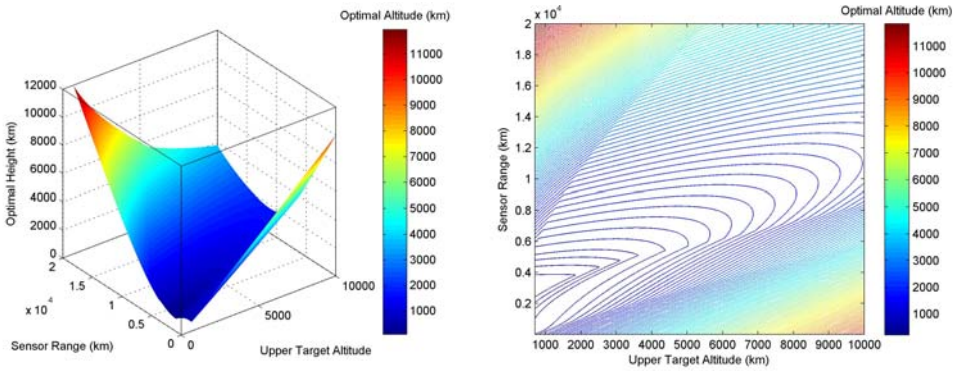

(a) (b)

Figure 17 - Sample Optimal Height Surface

CONCLUSIONS

The present study focuses on the identification of the optimal satellite altitude necessary to achieve maximum ATH coverage over an altitude limited band with atmospheric or environmental visibility constraints. Unlike earlier results regarding optimal BTH and ATH coverage, no direct correlation exists between the coverage angle and the maximum coverage area. The coverage area, in this case, is a nonlinear piecewise continuous function that requires special geometrical considerations. This investigation reveals that the key to computing the coverage area in this more complex case lies in the proper identification of the mutual intersections between the tangent line with the range shell, the upper target altitude shell, and the lower target altitude shell. Many special cases are identified and discussed in this study. The end result is a composite nonlinear objective function that relates the bounded ATH coverage area to the satellite altitude. Future studies, building on these results, will focus on optimal constellation design and the incorporation of other constraints, such as latitude band of interest.

ACKNOWLEDGEMENTS

This work was performed at The Aerospace Corporation. The authors would like to thank Bill Adams and Tom Lang, of The Aerospace Corporation, for their valuable input during the course of this investigation.

REFERENCES

1. Walker, J.G., “Satellite Constellations”, Journal of the British Interplanetary Society, Vol. 37., PP. 559-571, 1984.

2. Lang, T.J., “Optimal Low Earth Orbit Constellations for Continuous Global Coverage,” AAS/AIAA Astrodynamics Specialist Conference, Victoria, B.C., Canada, Aug. 16-19, 1993.

3. Rider, L., “Optimal orbital constellations for global viewing of targets against a space background,” Optical Engineering, Vol. 19, No. 2, 1980.

4. Kobel, C., “LOS, ATH, Same Theta Coverage Geometry,” The Aerospace Corporation, Internal Presentation. 5/26/2007.

5. Fewell, M.P. “Area of Common Overlap of Three Circles,” Maritime Operations Division, Defense Science and Technology Organization, Technical Note, DSTO-TN-0722.